JOURNAL OF Applied Polymer SCIENCE

Power Consumption in the Compacting Process of Polymer Particulate Solids in a Vane Extruder

Jin-Ping Qu,[1,2] Xiao-Qiang Zhao,[1,2] Jian-Bo Li,[1,2] Si-Qi Cai[1,2]

[1]National Engineering Research Center of Novel Equipment for Polymer Processing, South China University of Technology, Guangzhou 510641, China

[2]Key Laboratory of Polymer Processing Engineering of Ministry of Education, South China University of Technology, Guangzhou 510641, China

Correspondence to: J.-P. Qu (E-mail: jpqu@scut.edu.cn)

ABSTRACT: An innovational vane extruder made polymeric materials endure an elongation stress that was much larger than the shearing stress in the extrusion process. The operating principle of the vane extruder was completely different than that of conventional screw extruders. As the first stage of polymer processing in the vane extruder, the process of solids conveying was composed of feeding, compacting, and discharging. Most of the energy was consumed in the compacting process of polymer particulate solids in this stage. A mathematical model was developed to analyze the power consumption in the process. The model showed that the power consumption was mainly influenced by the structural parameters of the vane extruder, including the rotor diameter, eccentricity, and axial width of the vane unit. The analysis indicated that more energy was used to generate pressure in the vane extruder than in a screw extruder. The theoretical model was verified by the experimental results. © 2012 Wiley Periodicals, Inc. J. Appl. Polym. Sci. 000: 000–000, 2012

KEYWORDS: compression; extrusion; modeling; polymer extrusion; processing

Received 19 November 2011; accepted 12 January 2012; published online
DOI: 10.1002/app.36806

INTRODUCTION

An extruder is a typical machine used to melt polymeric materials for further processing. Extruders have been developing rapidly in the areas of high speed, high efficiency, low noise, and low power consumption. The power consumption of an extruder is an important technical index. It can be reduced after the operation principle of the extruder has been fully investigated. The subsection of an extruder from the feeding inlet to the point where polymers begin to melt is in general defined as the *solids-conveying zone*. The energy consumed in the solids-conveying zone is an important part of the total power consumption of an extruder. However, in comparison with the great amount of research on the power consumption of melt-conveying zones in extruders, much less attention has been paid to the power consumption of the solids-conveying zone.

The particulate-solids-conveying zone has a very important role in the performance of an extruder. Solids are not only conveyed forward in this section; more importantly, they are compressed to prepare for plasticizing and melting in the next section. In a continuous extrusion process, the stress history of particulate solids in the conveying zone has an important effect on the subsequent form and structure of the product, and it also simultaneously has a significant influence on the power consumption. Therefore, further study of the stress mechanism of particulate solids moving in the conveying zone will help us to determine how exactly energy is consumed in this process and to establish a model of power consumption. Furthermore, the model will helpful for determining ways to reduce power consumption.

The earliest appropriate mathematical model describing the mechanism of solids conveying was established by Darnell and Mol[1] in 1956, and it was based on solid static friction and static equilibrium. It is well-known that the Darnell–Mol model is in the form of a one-dimensional plug flow. In 1969, Schneider[2] revised the assumption of isotropic stress distribution in the Darnell–Mol model and obtained a more realistic stress distribution by assuming a certain ratio between the compressive stress in the down-channel direction and stresses in other directions. In 1972, Broyer and Tadmor[3,4] modified the Darnell–Mol model, considering the effects of the screw helix and

temperature variation. More recently, there have been many other refinements applied to the model by Chung,[5,6] Lovegrove and Williams,[7–9] and Zhu, Chen, and Fang.[10–12] Although the plug flow model has several shortcomings, it has provided a basis for many theoretical and experimental investigations of solids-conveying processes in screw extruders.

Reducing the power consumption of extruder has become an important research direction in recent years. Qu and coworders[13–15] introduced the pulsating electromagnetic force field to the extrusion process and reduced the overall power consumption of the extruder. One of the advantages of the novel vane extruder[16] introduced in this study is its energy savings, and this was verified experimentally. In the vane extruder, several vane plasticating and conveying units (VPCUs) composed a complete extrusion system. Polymer flow in a VPCU is volume transportation in essence, which is completely different than that in the channel of a conventional screw extruder. It was our objective in this study to describe the solids-conveying process in the vane extruder. On the basis of the stress distribution analysis, a mathematical model of power consumption in the solids-compacting process was set up. An analytical solution of the model was obtained and was examined experimentally. The theoretical and experimental results show that the power consumption in the compacting process of polymer solids in the vane extruder was influenced by the structural parameters of VPCU, the location of VPCU, and the friction coefficients between the polymer solids and interfaces of VPCU.

NOVEL VANE EXTRUDER

A conventional extruder is generally composed of a stationary barrel and a rotating screw. It conveys polymers forward by a dragging effect generated from the relative revolution between the barrel and the screw. It is well known that polymeric materials endure a shearing stress that is much larger than the elongation stress in the extrusion process in a conventional extruder. The other characteristic of the conventional extruder is that its production capacity is greatly affected by the die pressure. In many experiments, it has been found that the energy efficiency is very low in the particulate-solids-conveying process in conventional extruders. However, to achieve the purpose of melting and conveying polymers, there has been only one choice—a stationary barrel and a rotating screw.

In this study, a novel vane extruder was developed. The structure of the vane extruder is shown in Figure 1. The biggest difference between the vane extruder and a conventional extruder is that it has a rotor instead of a screw. The rotor is a circular shaft, and it is divided into several sections along the axial direction. There are two square grooves running through the rotor in every section, which are mutually perpendicular. Each groove is equipped with two vanes in pairs. The two vanes are in contact on their tops, and they can move in the groove under the push of external forces. The vane extruder has a stator instead of a barrel as in a conventional extruder. The rotor is installed eccentrically inside the circular hole of the stator. The eccentricity between the rotor's center and the stator's is intentional, and it can be adjusted in some conditions. The maximum value of the eccentricity is equal to the difference between the inner radius of the stator and the outer radius of the rotor. The transportation efficiency of the vane extruder is the highest when the eccentricity reaches its maximum. Also, there is a circular baffle at each end of each section of the rotor. Two adjacent vanes (which are 90° apart from each other along the circumferential direction), the inner surface of the stator, the outer surface of the rotor, and two circular baffles are encircled by a cylindrical chamber. Obviously, there are four cylindrical chambers between the two baffles along the axial direction of the rotor. These four cylindrical chambers as whole are called a VPCU.

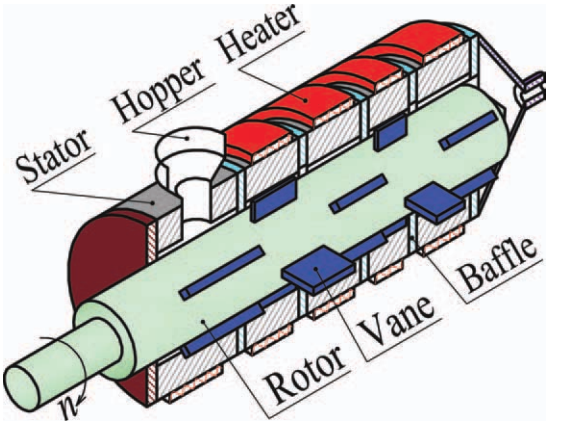

Figure 1. Schematic diagram of the vane extruder. [Color figure can be viewed in the online issue, which is available at wileyonlinelibrary.com.]

In brief, the vane extruder is composed of several VPCUs along the axial direction. When the rotor rotates, two pairs of vanes move back and forth in corresponding grooves. Simultaneously, the volume of each chamber changes periodically because of the eccentricity between the rotor's center and the stator's. On the one hand, polymeric materials will be charged in the chamber from the previous VPCU via the hole on the circular baffle when the volume of the chamber increases. On the other hand, the polymer will be discharged from the chamber and fed in the next VPCU when the volume of the chamber decreases. The circular holes of the stator of two adjacent VPCUs are eccentric with the rotor's center in opposite direction. If the eccentricity in the previous VPCU is on the left, the eccentricity in the next VPCU will be on the right. This makes the volume of the chamber in the previous VPCU decrease and the volume of the corresponding chamber in the next VPCU increase simultaneously. Polymeric materials can be discharged from the previous VPCU and fed in the next one smoothly with the rotation of the rotor.

It is obvious that the novel vane extruder transports polymeric materials depending on the periodic change of the volume of chambers in VPCUs. This implies that the principle of the process of conveying material in the vane extruder is volume transportation, and this is completely different from the principle in conventional screw extruders, which is based on drag-induced transportation. Theoretical analysis and experimental results

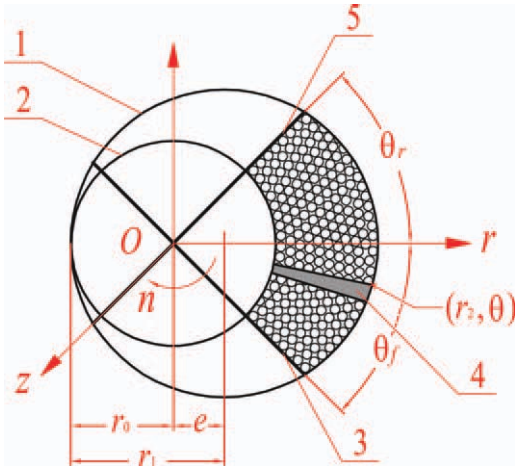

Figure 2. Schematic diagram of the solids-conveying zones: (1) stator, (2) rotor, (3) front vane, (4) differential element, and (5) rear vane. [Color figure can be viewed in the online issue, which is available at wileyonlinelibrary.com.]

showed that the vane extruder could reduce the thermomechanical history of a material in polymer processing. Thus, it had a high efficiency and a large output. Also, the size of the vane extruder was very small compared with conventional screw extruders.

DESCRIPTION OF THE SOLIDS-CONVEYING MODEL IN A VANE EXTRUDER

The vane extruder has some natural characteristics that are different from those of conventional extruders. A cross-sectional diagram of the solids-conveying zone in the vane extruder is shown in Figure 2. To simplify the solids-conveying process and allow for an analytical solution, some basic assumptions were needed, as follows:

1. The polymer solid particles in the chamber, which was encircled with a stator, rotor, vanes, and baffles, could be compressed, and there was no sliding between them.
2. The chamber was always filled with polymer solid particles when its volume changed with the rotation of the rotor.
3. The radial stress, axial stress, and circumferential stress changed only along the circumferential direction (the moving direction of the material).
4. The ratio of the normal stress to the circumferential stress (K) was constant, it was independent of position, and the change in the stress distribution in the material was neglected.
5. The angle θ_f was the angular coordinate of the front vane, and it changed with the rotation of the rotor. It could be used to represent the location of the chamber.
6. The material density was assumed to be constant when θ_f was unchanged. In other words, the density changed when the chamber followed the movement of the rotor to a different location, and the change in the density in the chamber was neglected.
7. The coefficients of friction between the polymer and the wall of the channel were constant, the relative motion and friction between the polymer solid particles and the vanes were neglected.
8. The gravity and the influence that the change of the material temperature brought were neglected.

Then, on the basis of the previous assumptions, the solids-conveying model of the vane extruder was obtained.

MATHEMATICAL MODEL

To better describe the movement of the polymer solids in the chamber, a mathematical model was developed for the cylindrical coordinate system. A differential element along the circumferential direction is depicted in Figure 3.

Because the movement of polymer solids in chamber is a uniform circular motion with the same angular velocity as the rotor, the torque balance of the differential element relative to the center of rotation can be obtained. Because pressure builds up along the circumferential direction, the torque balance is made on a differential increment along the circumferential direction.

The various forces acting on the differential element are illustrated in Figure 3. These forces can be expressed in terms of the coefficients of friction, local geometry, and the differential pressure increment.[17] For a nonisotropic stress distribution, these forces are as follows:

$$\begin{cases} F_{r1} = Kr_0 W\left(p+\frac{1}{2}dp\right)d\theta \\ F_{f1} = f_r \cdot F_{r1} \\ F_{r2} = K_{r2} W\left(p+\frac{1}{2}dp\right)d\theta \\ F_{f2} = f_s \cdot F_{r_2} \\ F_{\theta 1} - F_{\theta 2} = W(r_2 - r_0)dp \\ F_{z1} = F_{z2} = \frac{1}{2}K(r_2^2 - r_0^2)\left(p+\frac{1}{2}dp\right)d\theta \\ F_{f3} = F_{f4} = f_b \cdot F_{z1} \end{cases} \quad (1)$$

where F_{r1} and F_{r2} are the radial forces exerted on the differential element by the outer surface of the rotor and the inner surface of the stator, F_{z1} and F_{z2} are the axial forces exerted by the two baffles on both ends of the VPCU, F_{f1}, F_{f2}, F_{f3} and F_{f4} are the frictional retarding forces caused by the previous four forces, $F_{\theta 1} - F_{\theta 2}$ is the net force resulting from the circumferential pressure gradient, the constant K refers the ratio of the axial

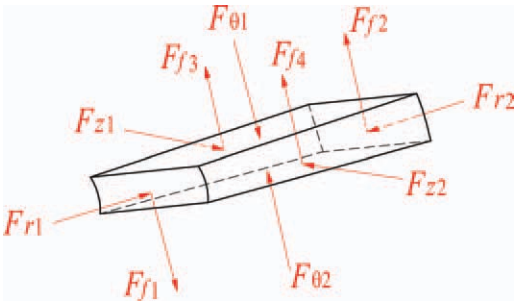

Figure 3. Forces acting on the differential element along the circumferential direction. [Color figure can be viewed in the online issue, which is available at wileyonlinelibrary.com.]

stress and radial stress to the circumferential (the moveable direction) stress, and f_r, f_s, and f_b are the frictional coefficients between the material and the surface of the rotor, the stator, and the baffles, respectively. In addition W is the axial width of the VPCU, r_0 is the outer radius of the rotor, r_2 is the radial coordinate of the point on the inner surface of the stator in the cylindrical coordinate system, whose origin is the center of the rotor.

The parameter r_2 is a function of the angular coordinate (θ), and it has the relationship with the inner radius of the stator (r_1) as follows:

$$r_2(\theta) = r_1 + e\cos\theta - \frac{e^2}{2r_1}\sin^2\theta \tag{2}$$

where e is the eccentricity between the rotor and the stator.

Because the chamber is always filled with polymer solids in the compacting process, as pointed out in the previously discussed assumptions, the motion of the differential element can be regarded as a pure rotation in the angular direction. Hence, a torque balance can be written in the circumferential direction by the calculation of the components of all of the forces in the corresponding direction as follows:

$$F_{\theta 1}\cdot\frac{r_0+r_2}{2} - F_{\theta 2}\cdot\frac{r_0+r_2}{2} + F_{f1}\cdot r_0 - F_{f_2}\cdot r_2 - (F_{f_3}+F_{f4})\cdot\frac{r_0+r_2}{2} = 0 \tag{3}$$

By the simplification of eq. (3), the following simple expression is obtained:

$$(F_{\theta 1} - F_{\theta 2} - 2F_{f3})\frac{r_0+r_2}{2} + F_{f1}r_0 - F_{f2}r_2 = 0 \tag{4}$$

The substitution of eq. (1) into eq. (4) and subsequent to considerable algebraic rearrangements, the following expression is obtained:

$$\left[-W(r_2-r_0)dp - Kf_b\left(p+\frac{1}{2}dp\right)(r_2^2-r_0^2)d\theta\right]\frac{r_0+r_2}{2} + KW\left(p+\frac{1}{2}dp\right)(f_r r_0^2 - f_s r_2^2)d\theta = 0 \tag{5}$$

where p is the pressure. Eliminating high order infinitesimal in eq. (5) and rearrangement, the expression is shown as

$$-\frac{W}{2}(r_2^2-r_0^2)dp = \left[\frac{Kf_b}{2}(r_2^2-r_0^2)(r_0+r_2) + KW(f_s r_2^2 - f_r r_0^2)\right]pd\theta \tag{6}$$

When the integral variables in eq. (6) are separated, the expression changes into the following form:

$$\frac{1}{p}dp = -K\left[\frac{f_b(r_0+r_2)}{W} + 2f_s + \frac{2(f_s-f_r)r_0^2}{r_2^2-r_0^2}\right]d\theta \tag{7}$$

The integration of eq. (7) after eq. (2) is substituted in it results in

$$p = p_f\cdot\exp\left\{\left[-\frac{Kf_b(r_0+r_1)}{W} + \frac{Kf_b e^2}{4Wr_1} - \frac{2K(f_s r_1^2 - f_r r_0^2)}{r_1^2-r_0^2}\right]\times(\theta-\theta_f) - \frac{Kf_b e}{W}\sin\theta - \frac{Kf_b e^2}{8Wr_1}\sin 2\theta\right\} \tag{8}$$

where θ_f is angular coordinate of the front vane of the VPCU in the cylindrical coordinate system and p_f is the pressure at the front vane.

Generally, two following expressions can be deduced:

$$\frac{Kf_b e}{W}\sin\theta << \theta \tag{9}$$

$$\frac{Kf_b e^2}{8Wr_1}\sin 2\theta << \theta \tag{10}$$

Therefore, the last two items of the exponent in eq. (8) can be ignored in reasonable tolerance. After they are eliminated, the following simple expression is obtained:

$$p(\theta) = p_f\cdot\exp[K_f(\theta_f-\theta)] \tag{11}$$

where

$$K_f = \frac{Kf_b(4r_1^2+4r_0r_1-e^2)}{4Wr_1} + \frac{2K(f_s r_1^2 - f_r r_0^2)}{r_1^2-r_0^2} \tag{12}$$

K_f is the coefficient used to calculate the pressure in VPCU chamber.

Equation (11) is the pressure expression in the chamber during the compacting and conveying processes of polymer solids. It indicates that the pressure distribution in the chamber is influenced by the geometrical parameters of the VPCU, frictional coefficients, K, and the pressure changes in the form of exponents along the circumferential direction.

RESULTS AND DISCUSSION

Pressure Distribution

It is well known from the previous pressure expressions that the pressure continuously varies along the circumferential direction in the chamber of the VPCU. In fact, polymer solids are pushed forward by the rear vane. With the rotation of the rotor, the volume of the chamber becomes smaller and smaller. The material in chamber will be compressed and will get denser and denser. Simultaneously, the material density becomes bigger, and the pressure builds up. However, the pressure is not equal everywhere in the chamber, and it reaches its maximum at the rear vane. On the contrary, it reaches its minimum at the front vane.

The exact value of pressure at a certain point in the chamber of the VPCU is determined by the minimum pressure. The minimum pressure is p_f, which can be deduced from the variation in the material density during the compacting process.

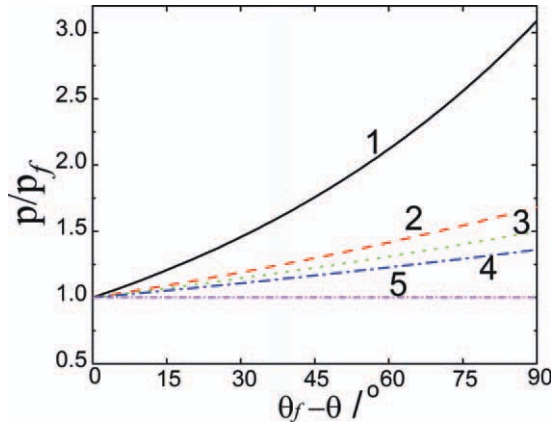

Figure 4. Influence of frictional coefficients on the pressure distribution in the chamber: (1) $f_b = 0.2$, $f_r = 0.2$, $f_s = 0.35$; (2) $f_b = 0.35$, $f_r = 0.2$, $f_s = 0.2$; (3) $f_b = 0.2$, $f_r = 0.2$, $f_s = 0.2$; (4) $f_b = 0.2$, $f_r = 0.35$, $f_s = 0.2$; and (5) $f_b = 0$, $f_r = 0$, $f_s = 0$. [Color figure can be viewed in the online issue, which is available at wileyonlinelibrary.com.]

The experimental work of Chung[5] indicated that the variation in the material density could be expressed by an empirical equation as follows:

$$\rho = \rho_m - (\rho_m - \rho_a) \cdot e^{-C_0 p} \tag{13}$$

where ρ is the material density, ρ_m is the material density at the utmost pressure, ρ_a is the material bulk density at atmospheric pressure, p is the pressure, and C_0 is a constant that is given by experimental data[18].

The expression of the pressure determined by the material density can be deduced from eq. (13) and is as follows:

$$p = \frac{\ln(\rho_m - \rho_a) - \ln(\rho_m - \rho)}{C_0} \tag{14}$$

On the one hand, the mass of the material is unchanged in the compacting process. On the other hand, the volume of the chamber decreases continually. These two factors lead to the increase in the material density.

Through analysis of the structure of the VPCU, shown in Figure 2, the expression of the volume of the chamber (V) can be obtained as follows:

$$V(\theta_f) = \left[\frac{\pi}{4}(r_1^2 - r_0^2) + r_1 e(\sin\theta_f + \cos\theta_f) + \frac{1}{2}e^2 \sin 2\theta_f\right] W \tag{15}$$

It can be seen that the volume of the chamber reaches its maximum when $\theta_f = \pi/4$. The maximum volume ($V_{\max}$) is as follows:

$$V_{\max} = \left[\frac{\pi}{4}(r_1^2 - r_0^2) + \sqrt{2} r_1 e + \frac{1}{2}e^2\right] W \tag{16}$$

The chamber fills with polymer solids when it reaches its maximum volume, and the material density is the bulk density (ρ_a). The material density increases to a new value when the volume of the chamber changes as $V(\theta_f)$. The new value of the density is as follows:

$$\rho(\theta_f) = \frac{V_{\max}}{V(\theta_f)} \rho_a \tag{17}$$

The minimum pressure in the chamber can be obtained by the substitution of eq. (17) into eq. (14). As we know from Figure 4, the minimum pressure is p_f, and its value can be obtained as follows:

$$p_f = \frac{\ln(\rho_m - \rho_a) - \ln(\rho_m - \rho(\theta_f))}{C_0} \tag{18}$$

The front vane is 90° ahead of the rear vane along the circumferential direction, which is

$$\theta_f - \theta_r = \frac{\pi}{2} \tag{19}$$

where θ_r is angular coordinate of the rear vane.

When eq. (19) is substituted into eq. (11), the pressure at the rear vane (p_r) can be obtained as follows:

$$p_r = p_f \cdot \exp\left(\frac{K_f \pi}{2}\right) \tag{20}$$

Substituting eq. (18) into eq. (11), the explicit expression of the pressure in the chamber can be obtained as follows:

$$p = \frac{\ln(\rho_m - \rho_a) - \ln\left[\rho_m - \frac{\nu_{\max}}{\nu(\theta_f)}\rho_a\right]}{c_o} \cdot \exp[k_f(\theta_f - \theta)] \tag{21}$$

From eq. (21), it can be seen that p is the function of the parameters θ_f and θ. The parameter θ_f can be used to represent the location of the chamber and $\theta_f - \theta$ refers to the relative position in the chamber. More precisely, eq. (21) indicates that the pressure in the chamber somewhere is determined not only by the position where it is located in the chamber but also by the location the chamber arrives at.

With $r_0 = 20$, $r_1 = 23$, $e = 3$, $W = 35$, and $K = 0.4$, Figure 4 was drawn according to eq. (21). Figure 4 shows that p_f is the minimum pressure in the chamber. The pressure increases gradually along the circumferential direction until it finally reaches its maximum at the rear vane. From Figure 4, another conclusion was obtained, that the variation of the frictional coefficient between the material and the stator surface (f_z) has greater influence on the pressure distribution compared with other two frictional coefficients, f_b and f_r. On the contrary, the variations of f_b and f_r had little influence on the pressure distribution in the chamber. Curve 5 in Figure 4 shows that the pressure can also be built up in the chamber even when there is no friction on all surfaces. The pressure will be equal that everywhere in the chamber under the hypothetical extreme condition.

With the aforementioned parameters and with all frictional coefficients equal to 0.2, $\rho_a = 0.52$, and $\rho_m = 0.92$, Figures 5 and 6

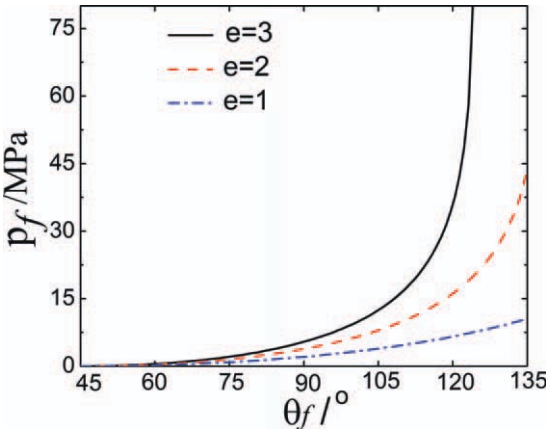

Figure 5. Influence of the eccentricity and angular location of the front vane on p_f. [Color figure can be viewed in the online issue, which is available at wileyonlinelibrary.com.]

were drawn according to eqs. (18) and (20). The value of C_0 used in the calculation was 5.39×10^{-8}/Pa, which was given by the experiment. Figures 5 and 6 show the effects of the eccentricity and θ of the vane on the pressure. It can be seen from Figure 5 that the pressure will be particularly large when $e = 3$ and $\theta_f > 120°$. There is a similar situation in Figure 6. The reason for the situation is that the compacting of the material reaches a limitation. Although it results in a large number in the theoretical calculation, the situation will not appear in a real compacting process. The polymer solids will be discharged before it reaches the compacting limitation. From Figures 5 and 6, a conclusion was obtained, that polymer solids are compressed in the compacting process because the volume of the chamber is gradually reduced, and pressure is built rapidly in the process. The pressure increases with increasing eccentricity and θ of the vane.

Total Power Consumption

The total power consumption can be obtained by three steps as follows. First, the power consumption of the rear vane pushing the materials forward should be calculated. Second, the power consumption of the front vane hindering the materials should be calculated. Finally, the power of the rotor dragging the materials forward should be calculated. The total power consumption is algebraic sum of the previous three parts.

The power of the rear vane working on the material (P_{Wr}) can be given as follows:

$$P_{Wr} = p_r \cdot W \cdot [r_2(\theta_r) - r_0] \cdot \frac{2n\pi}{60} \cdot \frac{r_2(\theta_r) + r_0}{2} \tag{22}$$

where $r_2(\theta_r)$ is the radial coordinate of the rear vane top and n is the rotational speed of the rotor.

The substitution of eq. (2) into eq. (22) leads the power of the rear vane pushing the materials forward to be expressed as follows:

$$P_{Wr} = \frac{n\pi W p_r}{60}\left[(r_1^2 - r_0^2) + 2r_1 e\cos\theta_r + e^2\cos 2\theta_r + \frac{e^4}{4r_1^2}\sin^4\theta_r\cos\theta_r\right] \tag{23}$$

Similarly, the negative power of the front vane working on materials (P_{Wf}) can be obtained as follows:

$$P_{Wf} = \frac{n\pi W p_f}{60}\left[(r_1^2 - r_0^2) + 2r_1 e\cos\theta_f + e^2\cos 2\theta_f + \frac{e^4}{4r_1^2}\sin^4\theta_f - \frac{e^3}{r_1}\sin^2\theta_f\cos\theta_f\right] \tag{24}$$

Thus, the net power provided by two vanes (P_{Wv}) can be obtained as follows:

$$P_{Wv} = P_{Wr} - P_{Wf} \tag{25}$$

The power of the rotor dragging the materials forward can be given as follows:

$$P_{Wro} = \int_{\theta_r}^{\theta_f} \frac{2n\pi}{60} r_0 \cdot f_r \cdot Kp(\theta) \cdot W \cdot r_0 d\theta \tag{26}$$

where P_{Wro} is the power provided by the rotor directly. The substitution of eq. (11) into eq. (26) and integration results in

$$P_{Wro} = \frac{2n\pi f_r r_0^2 r_1 W^2 (r_1^2 - r_0^2)(p_r - p_f)}{15 f_b (4r_1^2 + 4r_0 r_1 - e^2)(r_1^2 - r_0^2) + 120 W r_1 (f_s r_1^2 - f_r r_0^2)} \tag{27}$$

The total power consumption can be given as

$$P_W = P_{Wv} + P_{Wro} \tag{28}$$

where P_W is the total power consumption.

With $n = 60$ rpm and with the related parameters mentioned previously, Figures 7 and 8 were drawn according to eqs. (22)–(28). Figures 7 and 8 show that the power consumption increases gradually with the rotation of the chamber driven by the rotor. The rotation of the chamber is described by θ_f in the figures. The volume of the chamber decreases with the rotation, which leads to the increase of the pressure in the chamber and eventually results in the increase of the power consumption.

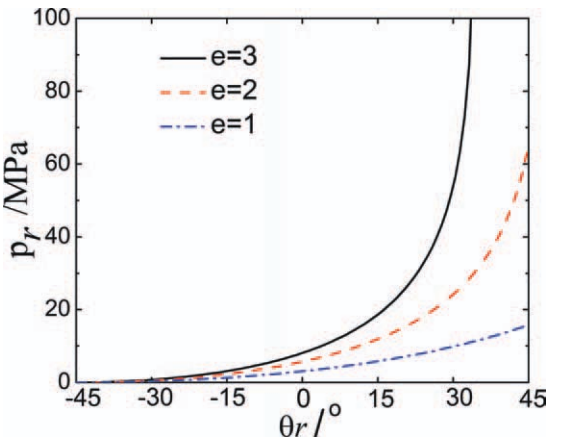

Figure 6. Influence of the eccentricity and angular location of the rear vane on p_r. [Color figure can be viewed in the online issue, which is available at wileyonlinelibrary.com.]

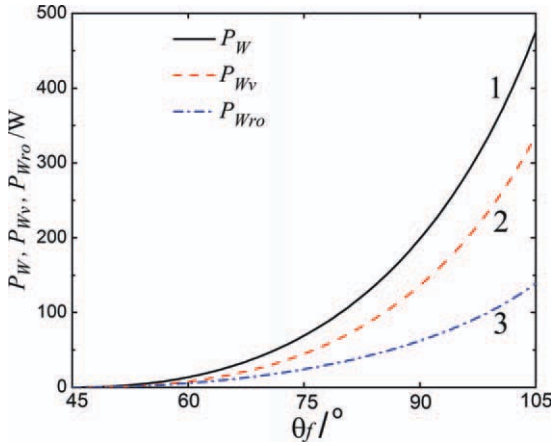

Figure 7. Variation of the power consumption with the angular location of the chamber: (1) total power consumption, (2) power provided by two vanes, and (3) power provided by the rotor directly. [Color figure can be viewed in the online issue, which is available at wileyonlinelibrary.com.]

Figure 7 shows that power provided by two vanes is greater than that provided by the rotor directly, especially in the case of the material being tightly compressed. The main reason for this situation is that the circumferential stress is the principal stress. Figure 8 shows that the total power consumption increases with the rise of the eccentricity, which is consistent with the conclusion that the pressure increases with the rise of the eccentricity, shown in Figures 5 and 6. In fact, a larger eccentricity can make the volume of the chamber decrease more quickly. The greater pressure in the chamber builds up in the process, and this results in a larger power consumption.

Dissipation Power

The total power introduced through the rotor and the two vanes is partly dissipated into heat at the surfaces of the stator and two baffles.

The power dissipated at the stator surface (P_{Ws}) is given by the product of the friction force and the relative velocity between the surface and the material. It can be obtained as follows:

$$P_{Ws} = \int_{\theta_r}^{\theta_f} \frac{2n\pi}{60} r_2 \cdot f_s Kp(\theta) \cdot W \cdot r_2 d\theta \tag{29}$$

Integration after the substitution of eqs. (2) and (11) into eq. (29) results in

$$P_{Ws} = K_{\theta 1} p_r - K_{02} P_f \tag{30}$$

where

$$K_{\theta 1} = \frac{n\pi K f_s W}{30}\left[\frac{r_1^2}{K_f} + \frac{2r_1 e}{1+K_f^2}(\cos\theta_f + K_f \sin\theta_f)\right] \tag{31}$$

$$K_{\theta 2} = \frac{n\pi K f_s W}{30}\left[\frac{r_1^2}{K_f} - \frac{2r_1 e}{1+K_f^2}(\sin\theta_f + K_f \cos\theta_f)\right] \tag{32}$$

$K_{\theta 1}$ and $K_{\theta 2}$ are the coefficients used to calculate the power dissipated at the inner surface of the stator.

The power dissipated at the surfaces of two baffles (P_{Wb}) is given by the product of the friction force and the relative velocity between the surfaces and the material. It can be obtained as follows:

$$P_{Wb} = 2\int_{\theta_r}^{\theta_f}\int_{r_0}^{r_2} \frac{2n\pi r}{60} \cdot f_b \cdot Kp(\theta) \cdot r d\theta dr \tag{33}$$

where P_{Wd} is the total dissipation power and r is the radial coordinate. Integration after the substitution of eqs. (2) and (11) into eq. (33) results in

$$P_{Wb} = K_{03} p_r - K_{04} p_f \tag{34}$$

where

$$K_{\theta 3} = \frac{n\pi K f_b}{45}\left[\frac{r_1^2 - r_0^3}{K_f} + \frac{2r_1 e}{1+K_f^2}(\cos\theta_f + K_f \sin\theta_f)\right] \tag{35}$$

$$K_{\theta 4} = \frac{n\pi K f_b}{45}\left[\frac{r_1^2 - r_0^3}{K_f} + \frac{2r_1 e}{1+K_f^2}(\sin\theta_f + K_f \cos\theta_f)\right] \tag{36}$$

$K_{\theta 3}$ and $K_{\theta 4}$ are the coefficients used to calculate the power dissipated at the surfaces of two baffles.

Thus, the total dissipation power can be given as follows:

$$P_{Wd} = P_{Ws} + P_{Wb} \tag{37}$$

Figure 9 shows the influence of the angular location of the chamber on the dissipation power. The dissipation power increases gradually with the rotation of the chamber; this is because the pressure increases gradually in the process. Also, the major component of the total dissipation power is the power dissipated into heat on the inner surface of the stator. The power dissipated at the interface of the material with the stator increases much faster than that dissipated at the interfaces of the material with two baffles in the compacting process.

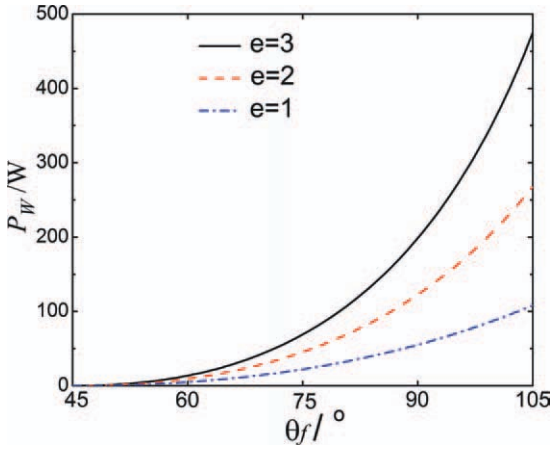

Figure 8. Influence of the eccentricity and angular location of the chamber on the total power consumption. [Color figure can be viewed in the online issue, which is available at wileyonlinelibrary.com.]

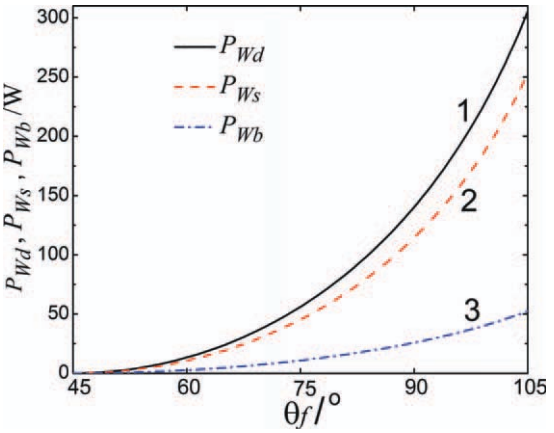

Figure 9. Influence of the angular location of the chamber on the dissipation power: (1) total dissipation power, (2) power dissipated on the stator surface, and (3) power dissipated at the surfaces of two baffles. [Color figure can be viewed in the online issue, which is available at wileyonlinelibrary.com.]

Power Consumption for the Building Pressure

The other part of the total power introduced through the rotor is used to generate pressure. It is obvious that the power consumption for pressurization (P_{Wp}) can be given as follows:

$$P_{Wp} = P_W - P_{Wd} \tag{38}$$

After eqs. (28) and (37) are substituted into eq. (38), the exact expression of the power consumption for pressurization in the chamber can be obtained as follows:

$$P_{Wp} = K_{06}p_r - K_{07}p_f \tag{39}$$

where

$$K_{05} = \frac{n\pi W(r_1^2 - r_0^2)}{60} + \frac{n\pi f_r r_0^2 W^2(r_1^2 - r_0^2)}{30f_b(r_1 + r_0)(r_1^2 - r_0^2) + 60W(f_s r_1^2 - f_r r_0^2)} \tag{40}$$

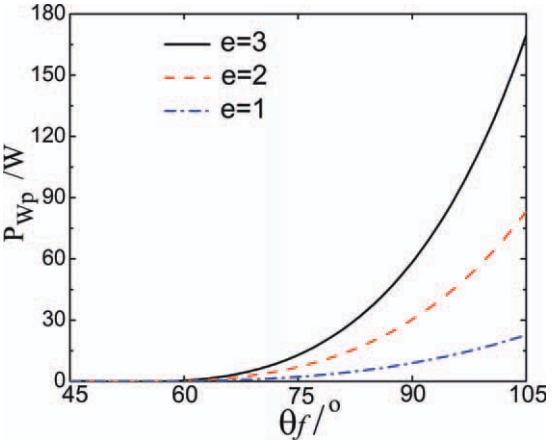

Figure 10. Influence of the eccentricity and angular location of the chamber on the power for pressurization. [Color figure can be viewed in the online issue, which is available at wileyonlinelibrary.com.]

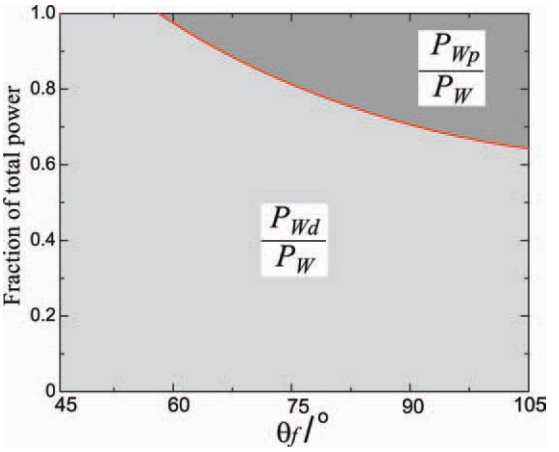

Figure 11. Graphical representations of the various components of the total power consumption. [Color figure can be viewed in the online issue, which is available at wileyonlinelibrary.com.]

$$K_{06} = \frac{n\pi W r_1 e\cos\theta_r}{30} + K_{05} - K_{01} - K_{03} \tag{41}$$

$$K_{07} = \frac{n\pi W r_1 e\cos\theta_f}{30} + K_{05} - K_{02} - K_{04} \tag{42}$$

K_{05}, K_{06} and K_{07} are the coefficients used to calculate power consumption for building pressure in VPCU chamber.

Equation (39) indicates that the power consumed for pressurization in the compacting process is not only a function of the pressures but also a function of geometrical parameters, the location of the chamber, and the friction coefficients. Figure 10 shows the influence of the eccentricity and angular location of the chamber on the power for pressurization. It can be seen that the power increases with the rise of the eccentricity and the rotation of the chamber, which is consistent with the increasing pressure in the process shown in Figures 5 and 6.

Figure 11 shows the various components of the total power consumption. From the figure, it can be concluded that most of the power is dissipated into heat, and the power used to generate pressure accounts for only a small part of the total power consumption. The power consumed for pressurization is close to zero in the initial stage, but it increases rapidly after the pressure builds up. It is worth mentioning that the maximum of the power consumed for pressurization is about 35% of the total power consumption, which is larger than the value of the same parameter in a conventional screw extruder.

EXPERIMENTAL

Equipment and Material

The self-developed experimental vane extruder had only one VPCU. The geometric parameters of the VPCU of the extruder are shown in Table I. The extruder discharged in the circumferential

Table I. Geometric Parameters of the Experimental Vane Extruder

r_0	r_1	W	Maximum eccentricity
20 mm	23 mm	35 mm	3 mm

Figure 12. Photograph of the VPCU chamber filled with solids. [Color figure can be viewed in the online issue, which is available at wileyonlinelibrary.com.]

direction, and it was equipped with visual glass at the axial end. Figure 12 shows the photograph of one side of the extruder, which was filled with polymer solids in its chamber.

The material used in this experiment was low-density polyethylene, and its physical characteristics are given in Table II.

Method

The experimental parameters were as follows:

1. The speed of the rotor was adjustable at 10 rpm.
2. The temperature was constant and was 100°C.
3. The eccentricity values were set as 1, 2, and 3.

According to the aforementioned parameters, the experiment was carried out as follows:

We made the rotor rotate and then stop at the point where the volume of the chamber reached the maximum;
We fed one chamber manually until the chamber was filled with polymer solid particles;
We kept the rotor rotate and collected the real-time torque through the torque sensor coaxial connected with the rotor.
We obtained the total power consumption by calculating the product of the torque and the rotational speed.

RESULTS

The curves shown in Figure 13 present the experimental results. The results show that most of the experimental value was close to the calculated value. In Figure 13, which compares all of the experimental curves, the same trend could be derived from these curves. This was that the experimental value of the total power consumption increased with the rotation of the rotor and the rise of the eccentricity; this was consistent with the trend shown by all of the calculated values.

Table II. Physical Characteristics of the Material Used in the Experiment

Material	ρ_m (g/cm^3)	ρ_a (g/cm^3)
Low-density polyethylene	0.92	0.52

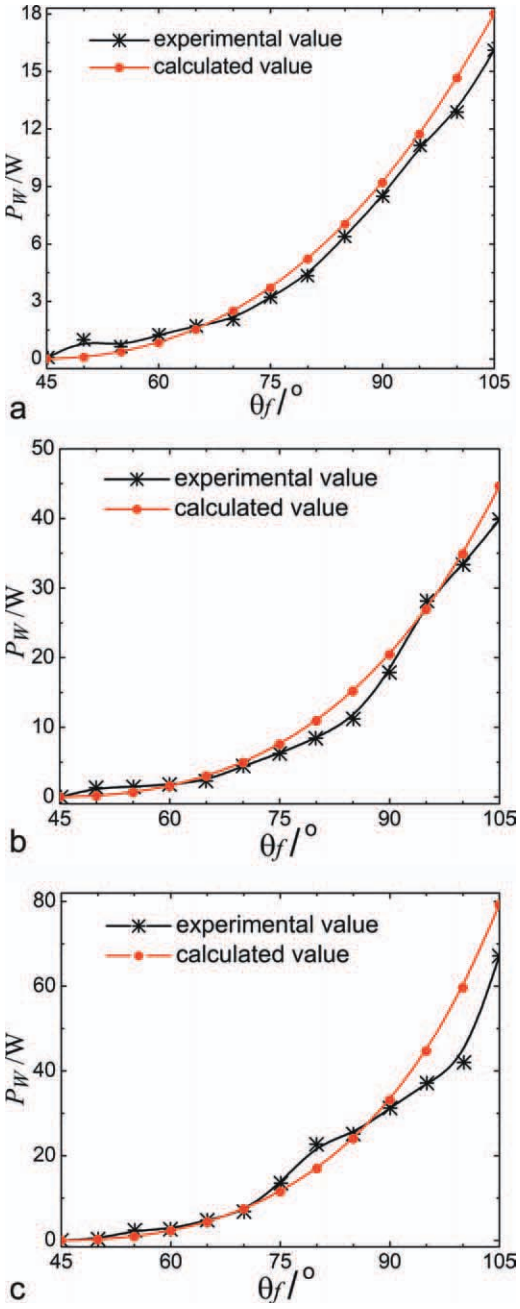

Figure 13. Relationship between the total power consumption and the location of the chamber: (a) $e = 1$, (b) $e = 2$, and (c) $e = 3$. [Color figure can be viewed in the online issue, which is available at wileyonlinelibrary.com.]

From Figure 13, we also found that experimental values of the total power consumption were usually smaller than calculated values, whether the eccentricity was large or small. Furthermore, the difference between the experimental values and the calculated values increased with the compacting process. The phenomenon was a result of more materials leaking into the latter chamber when the pressure increased. The pressure in the chamber increased in the compacting process. Simultaneously, the leakage of the materials increased in the process. However, the calculated values of the total power consumption were obtained under the assumption that there was no leakage.

CONCLUSIONS

By analyzing the aforementioned theoretical equations and experimental results, we drew the following conclusions:

1. The compacting process of polymer solids in the vane extruder is completely different than the solids-conveying process in a conventional screw extruder.
2. The pressure in the chamber is influenced by the location of the chamber, and it increases with decreasing volume of the chamber. The minimum value and the maximum value of the pressure are built at the beginning and the end of the chamber. The pressure in the chamber exponentially increases along the circumferential direction.
3. The power consumption is influenced by the structural parameters, the location of the chamber, and the frictional coefficients. The power consumption increases with decreasing volume of the chamber.
4. The majority of the power is provided by the vanes, and the rest is provided by the rotor directly.
5. Most of the power is dissipated into heat at the surfaces of the stator and baffles. The majority of the total dissipation power is dissipated into heat on the inner surface of the stator.
6. The power used to generate pressure accounts for a small part of the total power consumption. The maximum of the power consumed for pressurization in the vane extruder is larger than the value of the same parameter in a conventional screw extruder.

ACKNOWLEDGMENTS

The authors would like to acknowledge for the financial support of the National Natural Science Foundation of China (Grant No. 10872071, 50973035).

NOMENCLATURE

C_0	Constant.
e	Eccentricity between the rotor and the stator.
f_b	Friction coefficient between the material and the baffles.
F_{f1}	Frictional force on the rotor surface.
F_{f2}	Frictional force on the stator surface.
F_{f3}	Frictional forces on the rear baffle surface.
F_{f4}	Frictional forces on the front baffle surface.
f_r	Friction coefficient between the rotor and material.
F_{r1}	Radial force exerted by the rotor.
F_{r2}	Radial force exerted by the stator.
f_z	Frictional coefficient between the material and the stator surface.
F_{z1}	Axial force exerted by the rear baffle.
F_{z2}	Axial force exerted by the front baffle.
$F_{\theta 1}$	Circumferential force to promote the differential element.
$F_{\theta 2}$	Circumferential force to retard the differential element.
K	Ratio of the normal stress to the circumferential stress.
K_f	coefficient used to calculate pressure.
$K_{\theta 1}$, $K_{\theta 2}$	coefficients used to calculate power dissipated at stator surface.
$K_{\theta 3}$, $K_{\theta 4}$	coefficients used to calculate power dissipated at baffles surfaces.
$K_{\theta 5}$, $K_{\theta 6}$, $K_{\theta 7}$	coefficients used to calculate power consumption for building pressure.
n	Rotational speed of the rotor.
p	Pressure.
p_f	Pressure at the front vane.
p_r	Pressure at the rear vane.
P_W	Total power consumption.
P_{Wb}	Power dissipated at the surfaces of two baffles.
P_{Wd}	Total dissipation power.
P_{Wf}	Negative power of the front vane working on the material.
P_{Wp}	Power consumption for pressurization.
P_{Wr}	Power of the rear vane working on the material.
P_{Wro}	Power provided by the rotor directly.
P_{Ws}	Power dissipated at the stator surface.
P_{Wrv}	Power provided by two vanes.
r	Radial coordinate.
r_0	Outer radius of the rotor.
r_1	Inner radius of the stator.
r_2	Radial coordinate of the point on the stator surface.
V	Volume of the chamber.
$V_{\max}$	Maximum volume.
VPCU	Vane plasticating and conveying unit.
W	Axial width of the VPCU.
ρ	Material density.
ρ_a	Material bulk density at atmospheric pressure.
ρ_m	Material density at the utmost pressure.
θ	Angular coordinate.
θ_f	Angular coordinate of the front vane.
θ_r	Angular coordinate of the rear vane.

REFERENCES

1. Darnell, W. H.; Mol, E. A. J. *Soc. Plast. Eng. J.* **1956,** *12*, 20.
2. Schneider, K. Technical Report on Plastics Process in the Feeding Zone of an Extruder; Institute of Plastics Processing (IKV): Aachen, Germany, **1969.**
3. Broyer, E.; Tadmor, Z. *Polym. Eng. Sci.* **1972,** *12*, 12.
4. Tadmor, Z.; Broyer, E. *Polym. Eng. Sci.* **1972,** *12*, 378.
5. Chung, C. I. *Soc. Plast. Eng. J.* **1970,** *26*, 32.
6. Chung, C. I. *Polym. Eng. Sci.* **1975,** *15*, 29.
7. Lovegrove, J. G. A.; Williams, J. G. *J. Mech. Eng. Sci.* **1973,** *15*, 114.
8. Lovegrove, J. G. A.; Williams, J. G. *J. Mech. Eng. Sci.* **1973,** *15*, 195.
9. Lovegrove, J. G. A.; Williams, J. G. *Polym. Eng. Sci.* **1974,** *14*, 589.
10. Zhu, F.; Chen, L. *Polym. Eng. Sci.* **1991,** *31*, 1113.
11. Zhu, F. *Polym. Mater. Sci. Eng.* **1986,** *3*, 1.
12. Zhu, F.; Fang, S. *Polym. Mater. Sci. Eng.* **1987,** *4*, 22.
13. Qu, J. *Polym. Plast. Technol. Eng.* **2002,** *41*, 115.
14. Qu, J.; Cai, Y. *Plast. Technol. Eng.* **2006,** *45*, 1137.
15. Qu, J.; Zeng, G.; Feng, Y.; Jin, G.; He, H.; Cao, X. *J. Appl. Polym. Sci.* **2006,** *100*, 3860.
16. Qu, J. Chin. Pat. CN200810026054X (**2009**).
17. Tadmor, Z.; Gogos, C. G. Principles of Polymer Processing; Wiley: Hoboken, NJ, **2006**; p 484.
18. Qu, J.; Shi, B.; Feng, Y.; He, H. *J. Appl. Polym. Sci.* **2006,** *102*, 2998.